ELSEVIER

Journal of Nuclear Materials 265 (1999) 325–330

journal of nuclear materials

Letter to the Editors

Investigations of ion radiation effects at metal/liquid interfaces

M.B. Lewis *, J.D. Hunn

Oak Ridge National Laboratory, P.O. Box 2008, Bldg. 5500, Oak Ridge, TN 37831-6376, USA

Received 11 September 1998; accepted 10 November 1998

Abstract

Unique interactions of radiation effects and interfacial chemistry processes are possible when an energetic ion beam passes through the interface between a solid metal surface and a liquid. The purpose of this paper is to introduce a new ion beam method to investigate some of these effects. A liquid mercury target and a water target contained in a block with a steel foil window on one end have been irradiated through the foil with 2 MeV protons. The initial results for mercury show no interaction detectable above background; the initial results for water indicate radiation enhanced corrosion on the foil surface.

1. Introduction

The present design of the spallation neutron source (SNS) calls for a liquid mercury target contained in stainless steel, surrounded by a water cooled stainless steel jacket [1]. Protons with energy of approximately 1 GeV will pass through the stainless steel container walls before entering the liquid mercury. At the interface between the steel and the water and between the steel and the mercury, a unique radiation environment will be created. Irradiation of water with high energy protons (800 MeV) has recently been investigated for a spallation target at LANSCE [2]. While we do not have such high energy ions available at this laboratory, we have begun to investigate scaled down simulations in which MeV protons are used for the above two types of interfaces. In addition to the relevance of these irradiations to the SNS, similar kinds of radiation experiments are needed for other types of solid/liquid interfaces for a variety of applications. For example, these methods would be relevant to irradiation assisted stress corrosion cracking (IASCC) investigations for stainless steels in the core region of water reactors.

2. Background

2.1. Steel/mercury interface

Consider a proton beam passing through a steel window and emerging in a mercury target. The atomic binding energy in liquid mercury is considerably smaller than in solid metals; the surface atoms, for example, are bound by less than 1 eV ($\Delta H_{vap} = 0.6$ eV/atom). Even small momentum transfers from energetic protons to Hg atoms can cause these atoms to repel in any direction. Atoms moving against the line of direction of the proton beam can stop in the first few atomic layers of the steel window. Further inward diffusion of Hg into defects or along grain boundaries might significantly alter the mechanical properties of the window. Fig. 1 shows the result of a calculation [3] of this 'atomic mixing' near a liquid Hg/solid 316 stainless steel (SS) interface. In this example, chosen for its relevance to the present work, a 1.6 MeV H^+ beam with a fluence of 2×10^{21} H^+/m^2 passes through the 12 μm foil, emerging into the Hg with about 230 keV. This fluence creates about 0.045 displacements per atom (dpa) at the SS surface in contact with the Hg. In the first couple of SS monolayers, the concentration of Hg can reach a few at.%, the actual concentration depending strongly on the displacement energy, E_d, in Hg as well as linearly on the ion fluence.

* Corresponding author.

0022-3115/99/$ – see front matter
PII: S0022-3115(98)00885-X

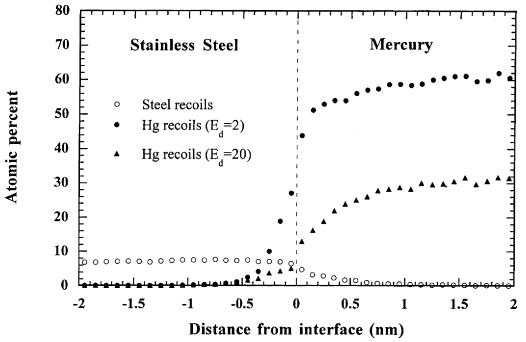

Fig. 1. Simulation (SRIM) of proton-induced atomic mixing at a 316 SS/liquid mercury interface. Mercury atoms recoil from the liquid and become implanted into the first few atomic layers of the steel below its interface with Hg. The simulation compares two displacement energies, E_d, in liquid Hg; the effective E_d probably lies between these values.

2.2. Steel/water interface

Consider the example above, but with the mercury replaced by water. The energy loss of the bombarding ions as they emerge from the window into the water creates a significant density of ionized water molecules or ion–electron pairs at the interface. During the time in which these ion-pairs form free radicals and attempt to reestablish chemical equilibrium through numerous reactions, the liquid at the region of the interface is in a high chemical-potential state and at an elevated temperature. Consider a 2.0 MeV incident H^+ beam passing through the same type of foil as above, but now it emerges into the water with an average energy of 990 keV; the ion range in the water would be about 2×10^4 nm. On average, for each molecule of H_2O dissociated into H and OH radicals, the protons would be expected to lose an amount of energy, E_B, of approximately 17 eV [4]. Thus a single ion track might generate more than 10^4 radicals within a distance of about 10^4 nm from the metal surface. The region near each ion track would be inhomogeneous in ion density [4]. Yet, a continuous flux of incident protons would result in an average concentration of radicals which would be much higher than that normally found in water and would persist, along with an elevated temperature, throughout the irradiation, if not longer.

In order to calculate the average radical concentrations [5], we take a simple form for the average H_2O bond scission rate as

$$S = \frac{f}{E_B N}\left(\frac{dE}{dx}\right), \tag{1}$$

where f is the ion beam flux, dE/dx the energy loss per unit length of ion track and N the bond density. We then solve the chemical recombination and reaction rate equations [5,6] using equations similar to those previously applied to aqueous radiation chemistry problems [2,4,6]. For this short communication, we limit the number of equations to the most essential among neutral species (Table 1). For each of the species (H, OH, etc.) an average concentration rate equation can be written; for example, the rate equation for the hydrogen concentration (H) would be

$$d(H)/dt = S - k_1(H)(OH) - 2k_2(H)^2 - k_4(H)(H_2O_2) - k_6(HO_2)(H), \tag{2}$$

where k_n are the various rate constants [7,8] from Table 1. The set of rate equations based on the reactions in Table 1 is given in Table 2. While these homogeneous concentration equations are only the limiting case for the more realistic inhomogeneous equations, important information can be obtained from them [5,9]. A more realistic, low energy ion-track model [10] will soon be applied to the present problem.

The solution of the rate equations for our experimental conditions in the first 0.01 s is shown in Fig. 2. It is immediately evident that the average concentrations of oxygen-bearing radicals increase rapidly. The presence of these molecules could increase the rate of oxidation, Eq. (3a), and metallic dissolution, Eq. (3b):

$$M + O_2 \rightarrow MO_2 \tag{3a}$$

$$M + OH \rightarrow M^+ + OH^-. \tag{3b}$$

3. Procedure

In order to investigate the above effects, we fabricated two of target blocks: one of nickel for good

Table 1
Rate constants for the primary chemical reactions of neutral species expected along energetic ion tracks in water

Reaction	Rate constant k (10^{10} l/mol/s)
Recombination reactions	
1. $H + OH \rightarrow H_2O$	2.4
2. $H + H \rightarrow H_2$	1.0
3. $OH + OH \rightarrow H_2O_2$	4.0
Product reactions	
4. $H + H_2O_2 \rightarrow H_2O + OH$	0.010
5. $OH + H_2O_2 \rightarrow H_2O + HO_2$	0.005
6. $HO_2 + H \rightarrow H_2O_2$	1.0
7. $HO_2 + OH \rightarrow H_2O + O_2$	1.0
8. $HO_2 + HO_2 \rightarrow H_2O_2 + O_2$	0.0002

These reactions are initiated from the dissociation of water molecules by their collisions with the ions. The rate constants are from Ref. [7,8].

Table 2
Rate equations for the chemical products from reactions listed in the Table 1

Product	Reaction rate
H	$d(H)/dt = S - k_1(H)(OH) - 2k_2(H)^2 - k_4(H)(H_2O_2) - k_6(HO_2)(H)$
H_2	$d(H_2)/dt = k_2(H)^2$
OH	$d(OH)/dt = S - k_1(H)(OH) - 2k_3(OH)^2 + k_4(H)(H_2O_2) - k_5(OH)(H_2O_2) - k_7(HO_2)(OH)$
H_2O_2	$d(H_2O_2)/dt = k_3(OH)^2 - k_4(H)(H_2O_2) - k_5(OH)(H_2O_2) + k_6(HO_2)(H) + k_8(HO_2)^2$
HO_2	$d(HO_2)/dt = k_5(OH)(H_2O_2) - k_6(HO_2)(H) - k_7(HO_2)(OH) - 2k_8(HO_2)^2$
O_2	$d(O_2)/dt = k_7(HO_2)(OH) + k_8(HO_2)^2$

S is defined in the text.

thermal conductivity and one of Lucite for visual observations. Each block had a small cavity, which together with an O-ring sealed foil window, could confine a liquid in a high vacuum environment. A schematic representation of the block is shown in Fig. 3. Cavity volumes were 1 or 2 ml. The cavity was filled with either water or mercury. In the case of water, we used isotopically enriched D_2 ^{16}O or H_2 ^{18}O to aid in the analyses to follow. The foils [11] investigated were austenitic (Fe–18Cr–10Ni–3Mo) and ferritic (Fe–9Cr–1Mo) steels with thickness of about 12 μm. Incident protons of 1.6 MeV (Hg case) or 2.0 MeV (water case) were expected to emerge at the foil/liquid interface with energies around 230 and 990 keV, respectively [3]. In the Hg case, this energy was directly measured with a charged particle detector as follows: A 1.632 MeV proton beam was backscattered from a carbon substrate coated with 1 nm of gold. This resulted in an energy spectrum, at 160° scattering angle, of nearly monoenergetic 1.6 MeV H^+ (backscattered from the gold) plus a continuum below 1.2 MeV (backscattered from the carbon substrate). This technique provided a particle flux low enough for the detector system (a direct accelerator beam would be too intense). The backscattered protons passed through the metal foil and were captured in the detector. Fig. 4 shows the measured energy spectrum pertaining to the 1.6 MeV incident protons. Fig. 4 also shows a SRIM simulation [1] for 1.6 MeV protons transmitted through 12.1 μm of 316 stainless steel. The excellent agreement between the two spectra lends support to the reliability of the simulation method used to obtain Fig. 1.

In both the mercury and water cases, the proton beam was defocused and collimated to give a 5 mm diameter spot of nearly uniform intensity at the target. Irradiations were made with a beam intensity of about 1×10^4–2×10^4 μA m^{-2} to fluences of 10^{21} or 2×10^{21} m^{-2} over a 4 h period. A thermocouple was placed in contact with the block to monitor the temperature which did not rise beyond 30°C. However, a thermocouple welded to the outside of the foil and exposed to the beam rose to about 80°C in the case of the water-filled cavity. Control experiments were also carried out in which the metal foil was left in contact with the liquid at room temperature and 90°C (with water) for 4 h without irradiation.

Gas created along the ion track in water was collected in a graduated cylinder via displacement of dis-

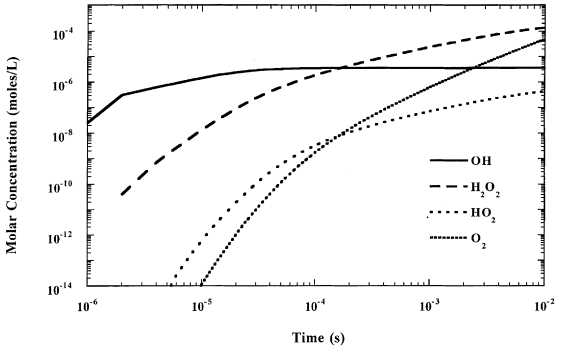

Fig. 2. The solution of the equations in Table 1 for the first 0.01 s of irradiation. The ion beam is 990 keV protons with a flux of 3.75 mA/m^2 in water.

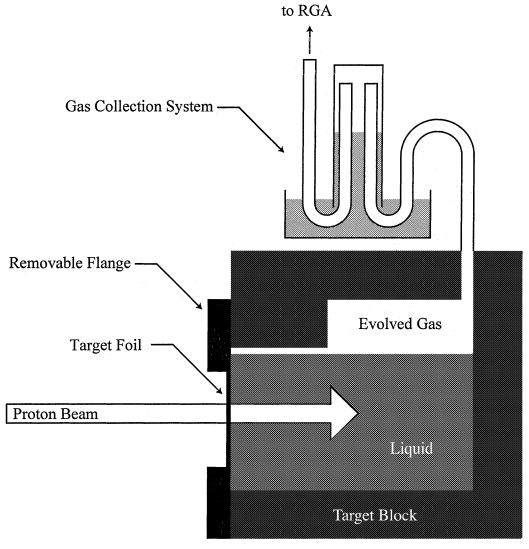

Fig. 3. A schematic representation of the target assembly. The proton beam passes through the foil from the left and enters the liquid with reduced energy.

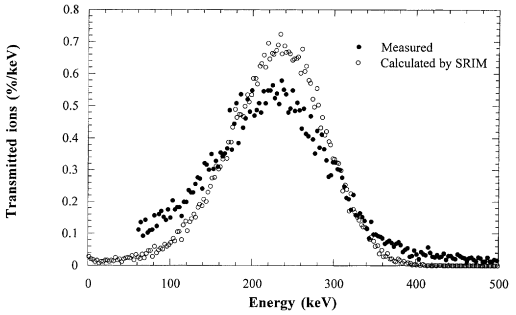

Fig. 4. Measured and calculated energy dispersion spectra following the passage of 1.6 MeV protons through a 12.1 μm thick SS foil.

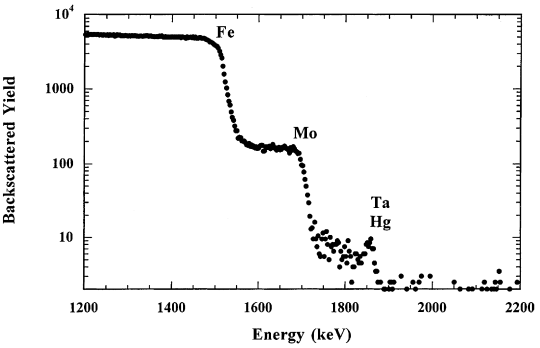

Fig. 5. Typical RBS spectrum of 2 MeV He^+ backscattered from the mercury-exposed steel foil before or after irradiation.

tilled water (shown schematically in Fig. 3). In this manner, the approximate volume of evolved gas could be measured. Following the irradiation, this gas was bled back into the vacuum system for residual gas or RGA mass analysis. In another experiment, the tubing was connected directly to the target chamber (instead of the graduated cylinder) and partially evacuated prior to irradiation. Then during irradiation the gas was bled into the chamber and analyzed in situ.

After irradiation, the target block was immediately removed from the target chamber and the foil was then removed from the block. The water was placed in a small sample bottle and analyzed for pH and for Ni and Fe ion concentrations. The foils were placed in a scattering chamber for ion beam analyses. Rutherford backscattering spectroscopy (RBS) was used to quantitatively measure the amount of mercury and elastic recoil detection (ERD) was used to measure the hydrogen or deuterium near the surface. The $^{16}O(d,p)$ and $^{18}O(p,\alpha)$ nuclear reactions were used to measure surface oxidation.

4. Results

4.1. Mercury

In the initial experiments, Hg droplets could be seen, with an optical microscope, to be trapped on the irradiated surface of the foil. The unirradiated foil in contact with Hg did not show trapping. SEM analysis determined that this trapping was due to carbon deposits from trace amounts of hydrocarbon impurities dissociated by the ion beam during irradiation. A second irradiation was carried out following more careful cleaning of the target and using distilled Hg; in this case no Hg was observed on the surface. Unfortunately, Ta inclusions were discovered on the foil surface by SEM. Due to the presence of Ta, which caused a background near Hg in the RBS spectra of Fig. 5, the sensitivity for detecting Hg was limited to about 50 appm. This concentration integrated over the approximately 100 nm of RBS sensitivity depth (i.e., the spectral region free of Mo background in Fig. 5) yields about 5×10^{17} Hg/m^2. This compares with the number 1.1×10^{18} Hg/m^2 of calculated recoils penetrating at least one atomic layer below the target surface for the choice of $E_d = 20$ eV in Fig. 1. It should be noted that diffusion and partial pressure considerations indicate that one monolayer of Hg on the surface or freely diffusing to the target surface from a few monolayers below would probably evaporate within 0.01 s at room temperature. Thus, we would expect to see only subsurface trapped Hg. More sensitive experiments using a higher fluence and a foil with lower background are now in progress.

4.2. Water

During irradiation with water, small gas bubbles near the foil (viewed through the Lucite block) appeared quickly while larger bubbles, a few millimeters in diameter, began to appear after a few minutes and continued at an approximately constant rate throughout the remainder of the irradiation. At the end of the irradiation, a volume of 5.6 ml of gas was collected. A mass analysis taken during the first few minutes of irradiation indicated a considerable increase in the partial pressure. In the irradiation with D_2O, D_2 (mass = 4) was observed promptly. In a similar irradiation, but with H_2 ^{18}O, $^{18}O_2$ (mass = 36) was observed at a slightly later time as shown in Fig. 6. The data in Fig. 6 imply that the water near the foil becomes saturated with hydrogen and oxygen within seconds of the commencement of irradiation. No other gases have as yet been positively identified. The mass analyses indicated a molecular gas ratio of hydrogen to oxygen of about 10. The final pH of the irradiated water was found to increase from 6.13 to 6.55. The Ni ion concentration, thus far measured only for the ferritic foil, was found to be 0.21 mg/l in the irradiated and 0.11 mg/l for the control liquid; this con-

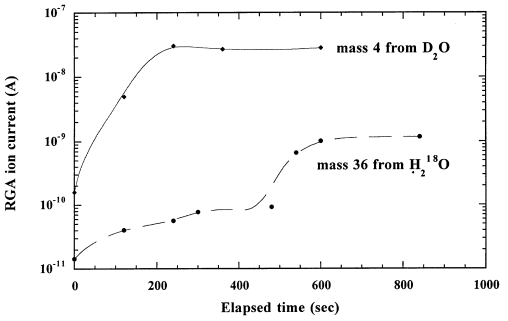

Fig. 6. Values of residual gas analysis (RGA) currents taken during the first few minutes of two separate proton irradiations. The mass, $M = 4$ or D_2 current from a D_2O target and $M = 36$ from a $H_2^{18}O$ target. Both liquids were contained in a Lucite block with a stainless steel foil window.

centration increase is presumably due to the reaction of the irradiated water with the Ni block. The Fe ion concentration was below 0.050 mg/l. More metallic ion concentration measurements are in progress.

ERD measurements showed about 0.3×10^{19} D/m^2 on the surfaces of both the irradiated and unirradiated foils due to a simple wetting. A spectrum of the $^{18}O(p,\alpha)$ reaction for one of the austenitic foils irradiated in the presence of H_2 ^{18}O is shown in Fig. 7. Approximately 100 atomic layers (7×10^{20} O/m^2) of oxide was observed for this irradiated specimen while the amount of oxygen found on the control specimens were about 5 atomic layers for the room temperature and 20 atomic layers for foil held at 90°C for 4 h. An examination of the surface by an optical microscope revealed a few small pits as deep as 0.01–0.1 μm and some flaking of surface layers not seen on the unirradiated foils.

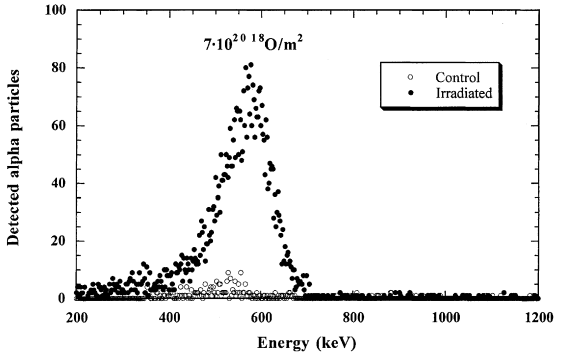

Fig. 7. Nuclear reaction $^{18}O(p,\alpha)^{15}N$ spectrum taken with $E_p = 700$ keV on the surface of a 316 SS foil exposed to water ($H_2^{18}O$) during proton irradiation. Also shown is an unirradiated (control) specimen.

5. Conclusion

We have explained why ion irradiation through metallic foils in contact with liquids could result in unique interactions of radiation effects and compatibility processes at the metallic surface. We then devised a controlled method to irradiate foil/liquid (mercury, water) targets and began to investigate such effects. Preliminary data were presented. In the mercury case, the nuclear recoil component of the ion–target collision should lead to Hg atoms being 'implanted' into the surface layers of the metal. However, the initial test was not sensitive enough to detect the Hg near the surface. In the water case, the data showed evidence for the rapid generation of oxygen in the liquid and enhanced oxidation and pitting of a stainless steel surface.

This work has demonstrated proof-of-principle for the above techniques. Such methods may now be employed to investigate the interactions of radiation effects and interfacial chemistry processes relevant to spallation neutron sources and water/reactor-core structures. Many other applications of the general technique are possible.

Acknowledgements

Research sponsored by the Division of Materials Sciences, US Department of Energy under contract number DE-AC05-96OR22464 with Lockheed-Martin Energy Research Corporation. The authors wish to acknowledge Dr Ed Kenik for the SEM measurements and Dr L.K. Mansur for helpful suggestions. We also wish to thank Drs Eal Lee, J.R. DiStefano and S.J. Pawel for technical review of the manuscript.

References

[1] L.K. Mansur, J.R. DiStefano, K. Farrell, E.H. Lee, M.S. Wechsler, in: Proceedings of the Topical Meeting on Nuclear Applications of Accelerator Technology, American Nuclear Society, 1997, p. 301.
[2] L.L. Daemen, G.S. Kanner, R.S. Lillard, D.P. Butt, T.O. Brun, W.F. Sommer, in: M.S. Wechsler, L.K. Mansur, C.L. Snead, W.F. Sommer (Eds.), Proceedings of the Symposium on Materials for Spallation Neutron Sources, Orlando, 1997, p. 83.
[3] J.F. Ziegler, J.P. Biersack, U. Littmark, The Stopping and Range of Ions in Solids, Pergamon, New York, 1985. Code: SRIM-98. The displacement energy, E_d, in Hg was taken as 2 and 20 eV for comparison, while 40 eV was used for steel.
[4] A. Chatterjee, J.L. Magee, J. Phys. Chem. 84 (1980) 3537.
[5] M.B. Lewis, E.H. Lee, L.K. Mansur, W.A. Coghlan, J. Nucl. Mater. 208 (1994) 61.

[6] G.V. Buxton, in: Radiation Chemistry, Farhataziz, M.J.A. Rodgers (Eds.), VCH, New York, 1987, p. 321.
[7] B.H.J. Bielsky, D.E. Cabelli, R.L. Arudi, A.B. Ross, J. Phys. Chem. Ref. Data 14 (1985) 1041.
[8] G.V. Buxton, C.L. Greenstock, W.P. Helman, A.B. Ross, J. Phys. Chem. Ref. Data 17 (1988) 513.
[9] W.G. Burns, R. Barker, Progress in Reaction Kinetics, ch. 7, vol. III, Pergamon, Oxford, 1965.
[10] M. B Lewis, W.A. Coghlan, J. Nucl. Mater. 228 (1996) 302.
[11] Foils were supplied by Goodfellow Cambridge Ltd.